REPORT DOCUMENTATION PAGE

Form Approved
OMB No. 0704-0188

1. REPORT DATE *(DD-MM-YYYY)*	**2. REPORT TYPE**	**3. DATES COVERED** *(From - To)*
03/01/2010	Final	04/01/2007 to 11/30/2009

4. TITLE AND SUBTITLE

Hybrid Nonlinear Optical Materials for Applications in Power Limiting and Photorefractive Devices

5a. CONTRACT NUMBER
FA9550-07-1-0307

5b. GRANT NUMBER

5c. PROGRAM ELEMENT NUMBER

6. AUTHOR(S)

Prasad, Paras N.

5d. PROJECT NUMBER

5e. TASK NUMBER

5f. WORK UNIT NUMBER

7. PERFORMING ORGANIZATION NAME(S) AND ADDRESS(ES)

SUNY at Buffalo
Natural Sciences Complex
Buffalo NY 14260

8. PERFORMING ORGANIZATION REPORT NUMBER

9. SPONSORING / MONITORING AGENCY NAME(S) AND ADDRESS(ES)

Research Foundation of SUNY
PO Box 9
Albany NY 12201

10. SPONSOR/MONITOR'S ACRONYM(S)

11. SPONSOR/MONITOR'S REPORT NUMBER(S)

12. DISTRIBUTION / AVAILABILITY STATEMENT

Distribution A - Unlimited Release

13. SUPPLEMENTARY NOTES

14. ABSTRACT

During the period covered by this project, our research efforts have been focused on the following subjects: i) designing and synthesizing highly multi-photon active organic chromophores, ii) exploring novel organic/inorganic composite materials and enhanced mechanisms for optical limiting applications, and iii) utilizing nano-technology to improve the performance of organic photorefractive materials working in IR wavelength range. Since 2008, we have successfully synthesized two groups of chromophores that exhibit high two-photon absorbability: one is a group of ladder-type oligo-*p*-phenylene cored chromophores useful for optical limiting; the other is a nitrosyl complex for light activated therapy through nitric oxide release. From the view-point of optical limiting applications, a solid two-photon absorbing material is much better than a solution or liquid medium, therefore we have developed a novel chromophore (AF289) doped polystyrene rod system, which manifests an excellent chemical/physical stability and provides a superior optical limiting and stabilization capability working with ~800-nm and ~160-fs laser pulses.

In respect to photorefractive study, our other recent achievement is the optimization of photosensitivity in hybrid nano-composites containing lead sulfide (PbS) nanoparticles (NPs) with optical activity in near-infrared (NIR) spectral range. To improve the optoelectronic properties, we have applied a ligand de-protection strategy to demonstrate a relative improvement in the efficiency of a charge generation of hybrid PR composites for PR applications. The resulting shortened ligands on NCs lead to enhancement of both photocurrent and diffraction efficiency in corresponding film devices. As a result, the photon generation quantum efficiency in photoconductivity study was improved to be over 20%, and the two-beam coupling (TBC) gain coefficient was pronounced as 173 cm^{-1}.

15. SUBJECT TERMS

16. SECURITY CLASSIFICATION OF:			**17. LIMITATION OF ABSTRACT**	**18. NUMBER OF PAGES**	**19a. NAME OF RESPONSIBLE PERSON**
a. REPORT	**b. ABSTRACT**	**c. THIS PAGE**			**19b. TELEPHONE NUMBER** *(include area code)*
U	U	U	Same as Box 12	36	

Standard Form 298 (Rev. 8-98)
Prescribed by ANSI Std. Z39.18

Final Report

(3/01/2010)

Hybrid Nonlinear Optical Materials for Applications in Power Limiting and Photorefractive devices

Prime Contract:

FA95500710307

Submitted by Prof. Paras N. Prasad

Institute for Lasers, Photonics and Biophotonics

State University of New York at Buffalo

Summary

During the period covered by this project, our research efforts have been focused on the following subjects: i) designing and synthesizing highly multi-photon active organic chromophores, ii) exploring novel organic/inorganic composite materials and enhanced mechanisms for optical limiting applications, and iii) utilizing nano-technology to improve the performance of organic photorefractive materials working in IR wavelength range. Since 2008, we have successfully synthesized two groups of chromophores that exhibit high two-photon absorbability: one is a group of ladder-type oligo-*p*-phenylene cored chromophores useful for optical limiting; the other is a nitrosyl complex for light activated therapy through nitric oxide release. From the view-point of optical limiting applications, a solid two-photon absorbing material is much better than a solution or liquid medium, therefore we have developed a novel chromophore (AF289) doped polystyrene rod system, which manifests an excellent chemical/physical stability and provides a superior optical limiting and stabilization capability working with ~800-nm and ~160-fs laser pulses.

In respect to photorefractive study, our other recent achievement is the optimization of photosensitivity in hybrid nano-composites containing lead sulfide (PbS) nanoparticles (NPs) with optical activity in near-infrared (NIR) spectral range. To improve the optoelectronic properties, we have applied a ligand de-protection strategy to demonstrate a relative improvement in the efficiency of a charge generation of hybrid PR composites for PR applications. The resulting shortened ligands on NCs lead to enhancement of both photocurrent and diffraction efficiency in corresponding film devices. As a result, the photon generation quantum efficiency in photoconductivity study was improved to be over 20%, and the two-beam coupling (TBC) gain coefficient was pronounced as 173 cm^{-1}.

CONTENTS

I. Synthesis, characterization, two-photon absorption and optical limiting properties of ladder-type oligo-*p*-phenylene cored chromophores

π-Conjugated organic molecules are an important class of multi-photon absorbing materials, which have attracted increasing attention due to their versatile applications in two-photon cellular imaging, optical power limiting, multi-photon pumped lasing, three-dimensional optical storage, and photodynamic therapy. Large two-photon absorption (TPA) cross-sections have often been associated with the extent of conjugation length (effective π-delocalization), which leads to an extended charge separation (a large π-conjugated system). Organic chromophores with large TPA cross sections are highly desirable for the exploitation of TPA processes at moderate laser intensities. In the past decade, a number of chromophores have been designed and characterized as highly two-photon active materials with TPA cross-sections up to several thousand GM (1 GM= 10^{-50}cm^4.s/photon). Recently, it has become clear that for the two-photon technology to realize its full potential, the development of more two-photon-active chromophores, which also possess other useful optical or chemical properties such as high fluorescence quantum yields, easy processability, good photo-stability and durability, will play a vital role. Although chromophores with extended conjugation length would have enhanced TPA due to their extended intramolecular charge transfer, they are often compromised with decreased fluorescence quantum yields and decreased photo-stability. Therefore, there is a need to develop novel materials, which may circumvent these trade-offs and concomitantly provide enhancement in TPA.

Fluorene is frequently used as an efficient building block for the construction of chromophores with high two-photon absorptivities, as well as excellent thermal and photochemical stabilities. Furthermore, truxene, a near-planar and highly fused structure, which comprises three fluorenes sharing a central benzene ring, was also found to be an excellent π-conjugated building block for two-photon active chromophores functionalized in three directions in space. From this viewpoint, linear ladder-type oligo-*p*-phenylenes, which formally consist of several "linearly overlapping" fluorenes would serve as an even better π-conjugated center in the design of a two-photon active chromophore, owning to their enhanced π-conjugation. An important parameter for enhancing π-conjugation is the molecular planarity because electronic interactions between conjugated π-orbitals and atomic orbitals of the main-group elements are maximized in a planar framework. Fixation of a π-conjugated system into a rigid and planar structure not only greatly facilitates the π delocalization, but also increases luminescence efficiencies, because such a structure can severely restrict geometric relaxations from the excited states. Thus, the use of a ladder-type π-conjugated motif is an efficient strategy for construction of a planar and rigid π-conjugated system, which may provide high TPA response with enhanced emission, as well as with increased thermal and chemical stabilities, because a simultaneous rupture of at least two bonds is necessary for complete scission of a ladder structure.

In this work, we first utilize several ladder-type oligo-*p*-phenylenes with various π-conjugation lengths for construction of the two-photon chromophores (Chart 1). As shown in Chart 1, these ladder-type oligo-*p*-phenylenes (from 1FL to 4FL) are flanked on both sides by two dibutylamino groups with (*E*)-1-styryl-4-vinylbenzene bridges. By systematically tuning the π -conjugation length of the planar core, an attempt to correlate the property/conjugation length relationship and to understand the structure-property relations is made.

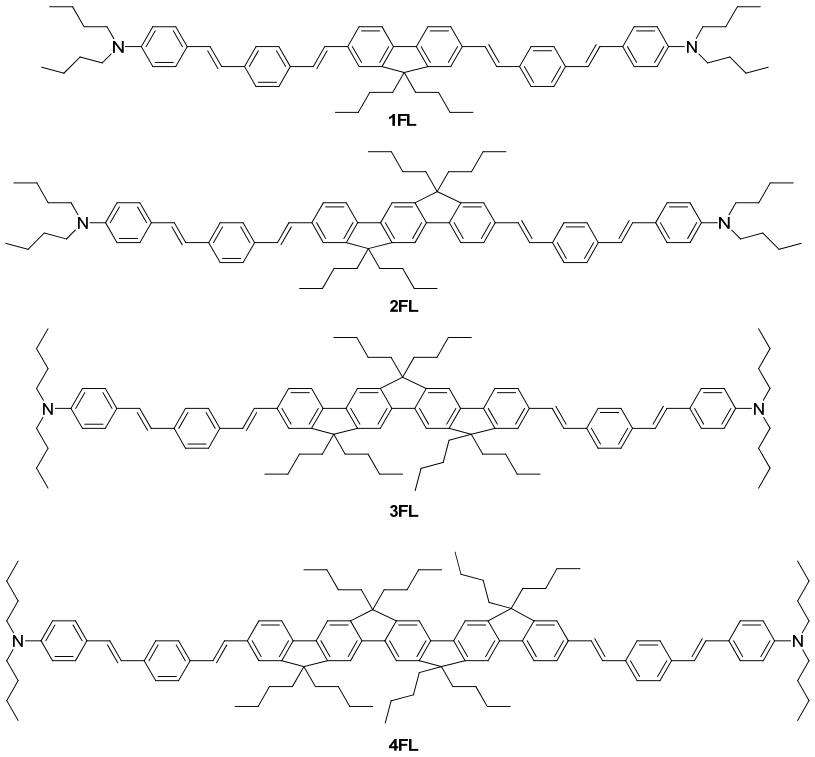

Chart 1. Molecular structures of two-photon absorbing chromophores containing ladder-type oligo-*p*-phenylenes (**1FL, 2FL, 3FL, 4FL**).

In discerning the structure/optical-properties relationship, it is informative to compare the absorption and emission spectra of compounds 1FL-4FL in the same solvent, and to study the solvent effects by comparing the absorption and the emission spectra of each chromophore in different solvents. The linear absorption and the fluorescence spectra for compounds 1FL-4FL in chloroform are shown in Fig.1.1, where a bathochromic shift in linear absorption was found in going from 1FL to 2FL, to 3FL, to 4FL. For example, 1FL has an absorption maximum at 422 nm, while 4FL has an absorption maximum at 450 nm. This gradual red-shift trend for these chromophores is due to their incrementally extended π-conjugation when the length of the ladder-type oligo-*p*-phenylenes becomes longer and longer. For a ladder-type oligo-*p*-phenylene cored chromophore with a longer conjugation length, to a higher extent it resemble the behavior of ladder-type materials, which have a rigid planar ladder structure leading to hindered geometrical (*viz*. vibrational and rotational) relaxation. The linear absorption spectra for compounds 1FL-3FL show no or little vibrational structure. However, the absorption spectrum for compound 4FL shows four apparent vibrational structures, probably due to its more nonpolar alkyl chains, which may disturb the solvent-chromophore interactions. Linear absorption and emission spectra for these chromophores in common solvents other than chloroform are also measured, and their linear absorption maxima, emission maxima are listed in Table 1-1. Other photophysical properties of these chromophores, including molar extinction coefficients, Stokes shifts, and fluorescence quantum yields are also summarized in Table 1-1. The values reported in this table are the average values of multiple (generally 3), fully independent measurements.

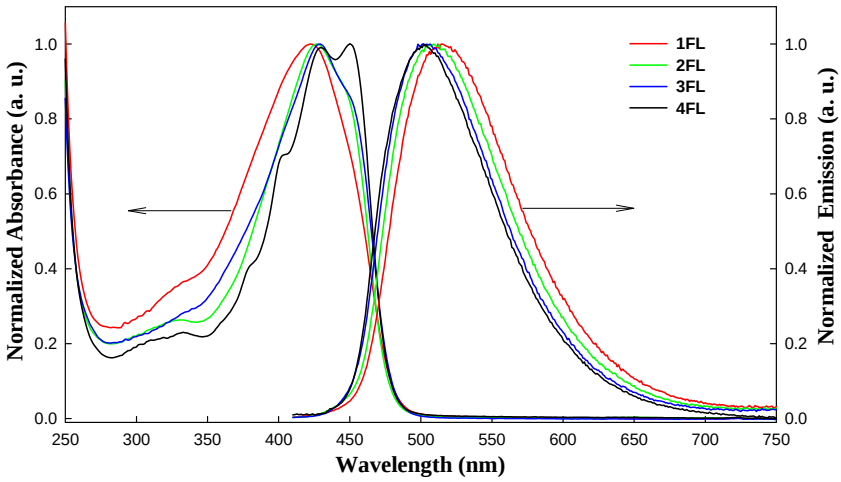

Fig. 1-1 Linear absorption and emission spectra for compounds 1FL-4FL in chloroform.

It is noteworthy that the absorption spectra, particularly the molar absorption coefficients, are hardly affected by solvent polarity. The linear absorption maxima are slightly red-shifted in solvents with intermediate polarities such as CH_2Cl_2, THF, and chloroform, compared to those in a less polar solvent such as cyclohexane. The longest linear absorption maxima wavelengths for these chromophores are observed in dimethylacetamide (DMA), a more polar solvent. This is consistent with the generally observed behaviors of quadrupolar chromophores. However, the fluorescence spectra and fluoresence quantum yield can be more strongly affected by solvent polarity. The linear absorption at maxima for compound 1FL in different solvents are in the range of 420-429 nm, and fluorescence peak of 1FL in THF is almost the same as that in $CHCl_3$. However, the fluorescence peak for compound 1FL shows a red shift of about 47 nm in solvents going from THF to DMA, and a blue shift of about 80 nm in solvents going from THF to cyclohexane.

In general, all these four chromophores have relatively high fluorescence quantum yields of 0.23-0.85 in six different solvents. There is a gradual increase of the fluorescence quantum yields with an incremental increase of π-conjugation length for these chromophores in chloroform: 1FL (0.59), 2FL (0.64), 3FL (0.69), and 4FL (0.75). Their fluorescence quantum yields in other solvents also follow this trend. For example, in DMA, their fluorescence quantum yields are in the order of: 4FL (0.52) > 3FL (0.37) > 2FL (0.28) > 1FL (0.23). The average fluorescence quantum yield enhancements in six solvents, from 1FL to 2FL, from 1FL to 3FL, and from 1FL to 4FL, are 116%, 129% and 154%, in that order. It is quite surprising to find that in polar solvents such as DMA, compound 4FL still has a relatively high fluorescence quantum yield, compared to compound 1FL. For example, the fluorescence quantum yield for compound 1FL in DMA is 0.23, indicating a drop of (0.34/0.57=0.60) 60% from the value in cyclohexane (0.57). However, only a (0.25/0.77=0.32) 32% decline in the fluorescence quantum yield for compound 4FL is recorded, when the solvent is DMA (0.52) instead of cyclohexane (0.77). It appears that both the increased backbone rigidity and conjugation are responsible for these observations. However, this is counter-intuitive as greater molecular planarity should actually encourage intermolecular stacking, which has been well established to be the main cause for

intermolecular fluorescence quenching. We speculate that in a highly polar environment, the nonpolar alkyl chains would curl back toward the conjugated backbone, forming a protective barrier against other approaching molecules from imparting emission quenching.

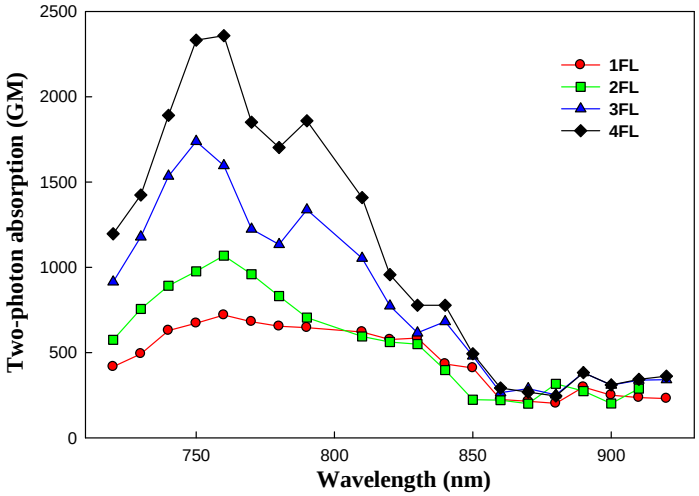

Fig. 1-2 TPA spectra for compounds 1FL-4FL in chloroform. The TPA cross sections (σ_2) were determined by using the two-photon excited fluorescence method relative to Coumarin 307.

The TPA spectra were determined by using laser pulses (~ 120 fs duration, 76 MHz repetition rate, ~ 2 nJ/pulse) from 715 to 940 nm generated by a mode locked Ti:sapphire laser (Mira from Coherent). A spectrum analyzer (IST-rees) was used to monitor the excitation wavelengths. All data were taken by two-photon-excited fluorescence method with Coumarin 307 (100 μM solution in methanol) as a reference. The measured TPA spectra for these chromophores are shown in Fig. 1-2. As shown in Fig. 1-2, the TPA cross-section peak values for chromophores **1FL-4FL** are 720, 1068, 1738, and 2357 GM, respectively. Hence, one may find in Fig. 1-2 that, the TPA cross-section peak value increases by a factor of 1.48, 2.41 and 3.27 when going from **1FL**, to **2FL,** to **3FL** and to **4FL**, in that order. This gradual enhancement in TPA for this series of chromophores can be attributed to the lengthening of the π-conjugated system.

From the TPA spectra, one may find that the TPA values for compounds **1FL, 2FL, 3FL, 4FL** in $CHCl_3$ at 775 nm are 667, 890, 1180 and 1777 GM, in that order. However, by using the nonlinear transmission method, their values are 512, 670, 970 and 1401 GM in $CHCl_3$, respectively. The values measured by the fluorescence method are 22-33% larger than those measured by using the nonlinear transmission method. This difference may be due to the different methods and different reference TPA chromophores that we used here. However, we have only relied on the results obtained by the same method for studying the structure/property relationships of the chromophores investigated in this work.

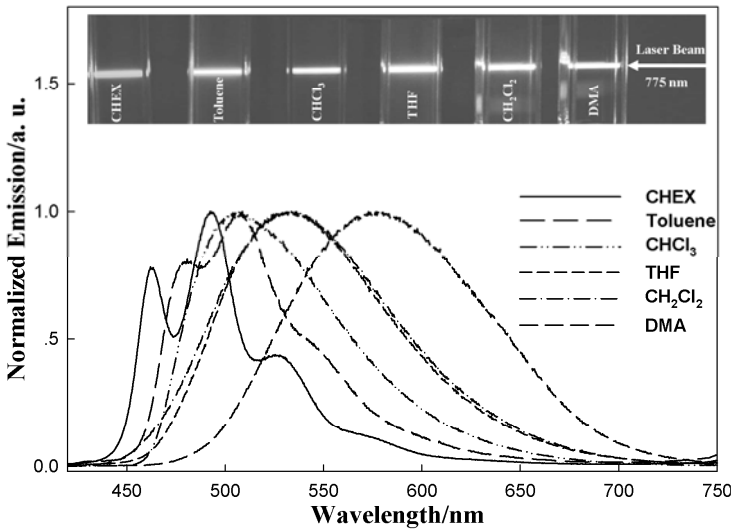

Fig. 1-3 Two-photon excited fluorescence for compound 3FL in solvents ($1.6*10^{-4}$ M) with various polarities, (inset) picture of two-photon fluorescence of compound 3FL in different solvents excited by a 775 nm laser beam.

Figure 1-3 depicts the TPE fluorescence for compound 3FL in six different solvents. The inset of Fig. 1-3, shows picture of TPE fluorescence of compound 3FL in different solvents irradiated by an unfocused 775 nm laser beam (Ti:sapphire laser/amplifier system, CPA-2010 from Clark-MXR, 160 fs, 1 kHz,). The divergence angle and input energy of the laser beam through a 1-mm pinhole were ~0.25 mrad, and 50 μJ, respectively. As a result of the large TPA cross-section values and the high fluorescence quantum yields of compound 3FL, two-photon excited fluorescence can be easily observed even with an unfocused laser beam. Compound 3FL exhibits a major change in emission color on changing of the solvent polarity. As shown in Fig. 1-3, blue emission was found for compound 3FL in the low-polarity solvent (cyclohexane), green emission was found for compound 3FL in solvents THF and $CHCl_3$ with moderate high polarities, while red emission was observed in a high-polarity solvent, DMA. These chromophores are promising for uses as environment sensitive TPE fluorescence probes, considering the sensitivity of their fluorescence on environment polarity, their strong TPA in the IR range and high fluorescence quantum yields. TPE will provide an intrinsic 3-dimentional resolution, which is unobtainable by single photon excitation.

For some laser-based applications such as optical communication, optical fabrication and manufacturing, the intensity or energy stability of the utilized laser beam is important. This is because random intensity or power fluctuation may be troublesome, especially from the standpoint of reproducibility, for these applications. However, a strongly multi-photon absorbing medium could be one of the approaches to reducing such fluctuation and stabilizing the pulsed laser signals. Since these chromophores have relatively large TPA at 775 nm, we investigated the relationship between the output intensity and the input intensity using these four chromophores. All the chromophores were dissolved in chloroform and the concentrations for chromophores **1FL-4FL**, were fixed at 0.005 M/L. Nonlinear optical transmission measurements were performed using 10 mm thick cells, with a Ti:sapphire laser generating output pulses of 160 fs duration and 775 nm wavelength.

The measured input and output intensity data for these chromophores are plotted out in Fig. 1-4. As shown in the figure, all these four chromophores show an optical limiting behavior. From the characteristic curves in Fig. 1-5, one can see why a two-photon absorbing medium can

be used to stabilize the laser pulse fluctuation. When the input energy increased from 0.21 J to 4.6 J (~21.9 times increase), the transmitted energy changed from 0.18 J to 2.03 J (~11.3 times increase) for compound **1FL**, from 0.17 J to 1.74 J (10.2 times increase) for compound **2FL**, from 0.17 J to 1.5 J (8.8 times increase) for compound **3FL**, and from 0.17 J to 1.25 J (~7.5 times increase) for compound **4FL**. These are typical optical limiting behaviors based on TPA mechanism. The optical limiting ability decreases in this order: **4FL** > **3FL** > **2FL** > **1FL**. Thus, if we use compound **4FL** as a two-photon absorbing medium to stabilize the input laser, we would expect that more than two-fold reduction in laser fluctuation may be achievable. However, we should point out that there is a saturation point in two-photon absorption observed for these chromophores at a certain light intensity for each chromophore. For example, for compound **2FL**, the experimental data deviate from the TPA fitting curve when the photo-energy flux is greater than 210 GW/cm^2.

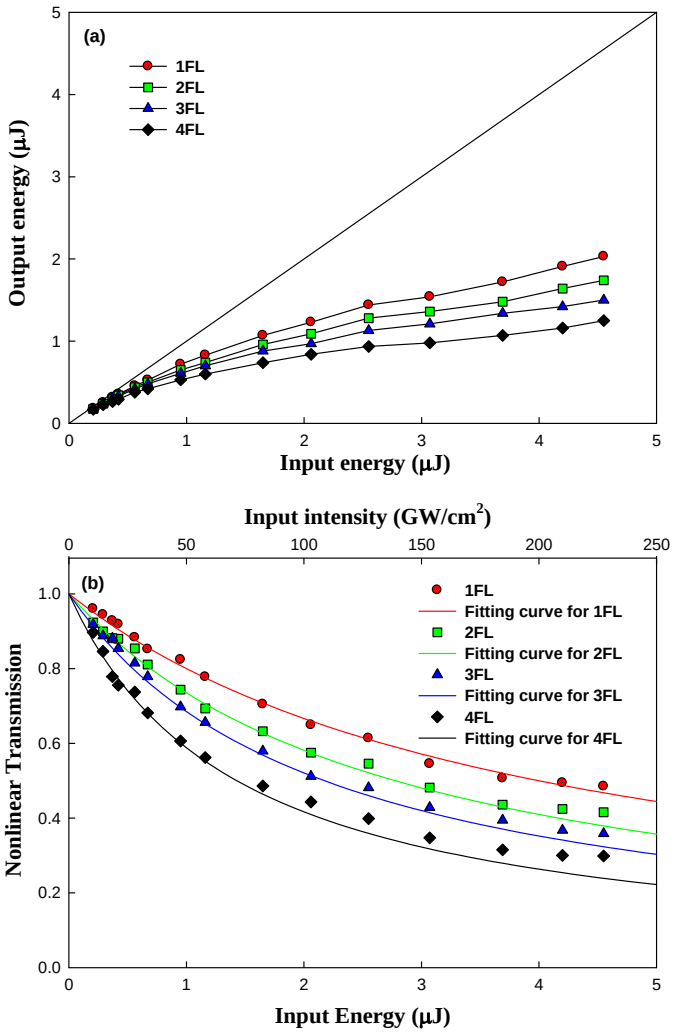

Fig. 1-4 Measured output intensity versus input intensity of the 775 nm laser pulses based on chromophores 1FL-4FL; The dash-dotted line represents the best fitting curve with TPA coefficient

values of β = 0.0601 cm/GW (1FL), β = 0.0787 cm/GW (2FL) and β = 0.114 cm/GW (3FL), and β = 0.165 cm/GW.

II. A water soluble two-photon absorbing nitrosyl complex for light activated therapy through nitric oxide release

In recent years, increasing attention has been paid to research on Nitric Oxide (NO) releasing materials (or NO donors), by virtue of the multiple roles playing by NO in biological processes, such as regulation of blood pressure, inhibition of tumor growth, and immunological self-defense. As one of the smallest biologically active molecules, cellular NO in nature is almost exclusively generated via a five-electron oxidation of L-arginine, which is catalyzed by NO synthases. However, in laboratory, researchers have developed and utilized a number of NO releasing materials such as furoxans, organic nitrite, nitrate, metal nitrosyl complexes and other nitro compounds. Many of the currently used NO donors such as 1-hydroxy-2-oxo-3-(aminoalkyl)-1-triazenes and 4-alkyl-2-hydroxyimino-5-nitro-3-hexenes are reagents that release NO by spontaneous autolysis. Compared to this spontaneous thermally activated NO release, materials with light-controlled NO release stand out as the most promising NO donors, due to the ease of manipulation by light, together with the fast response of the photochemical reactions. Furthermore, light-controlled NO releasing materials may allow a precise spatial and temporal control of NO delivery. Ford et al. have developed some thermally stable metal nitrosyl complexes which can be triggered photochemically to release NO on demand (as shown in Fig. 2-1). As shown in Fig. 2-1, 4 equiv. of NO is released per mole of metal nitrosyl cluster upon photodecomposition. They have successfully incorporated some chromophores (such as fluorescein, AF343) into the backbone of the Roussin's red salt esters. NO was qualitatively demonstrated to be photochemically produced via one-photon excitation, through the use of an NO-specific electrode. They showed that when a chromophore is incorporated into the Roussin's red salt esters, its two-photon absorptivity is retained. For biological applications, it is necessary to make these materials water soluble and bio-compatible.

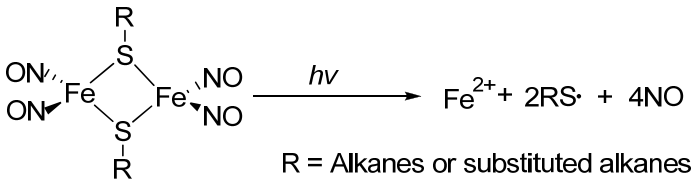

Fig. 2-1. Scheme for photochemical decomposition of a nitrosyl complex

As we know, two-photon techniques in biological applications hold the advantages of a better signal-to-noise ratio due to the reduction of autofluorescence often generated by UV or visible light, and the deeper tissue penetration at the two-photon excitation wavelength in the near IR. In recent years, NO donors that provide NO upon exposure to light have drawn special attention because of their utility in photodynamic therapy (PDT) for selected types of cancer. PDT is a noninvasive method of treating malignant tumors and age-related macular degeneration. Current practice of PDT is limited to a few functionalized porphyrins, and some other non-porphyrin photosensitizers, which may generate singlet oxygen ($^1O_2$) upon light irradiation.

Therefore, there is a significant interest in developing novel and more efficient sensitizers for use in PDT. NO releasing materials may be another class of promising sensitizers for PDT application, besides those materials generating singlet oxygen.

A series of oligo-phenylene vinylenes (OPVs) with comparatively large two-photon absorption (TPA) cross-sections have been prepared. The TPA cross-section values for these OPVs, increase with an increase in the π-conjugation length and the degree of intramolecular charge-transfer upon excitation. However, these compounds are barely soluble in water, which is a basic requirement to be suitable for biological applications. Therefore, there is a need to introduce water-soluble functional groups (such as oligo(ethylene glycol)) into the OPV backbone, resulting in materials with large TPA together with good water solubility. As shown in Fig. 2-2, three groups of tetra(oligo(ethylene glycols)monomethyl ether) make compound **2P-I** highly water soluble, while the iodoalkyl group at the other end can be used to link to a Roussin's red salt ester, resulting in the final targeted NO releasing Roussin's red salt complex (**2P-M**). As shown in Scheme 1, the water soluble metal nitrosyl complex was obtained by reaction between a two-photon absorbing chromophore (**2P-I**) and the Roussin's red salt,[25] with 36 % yield.

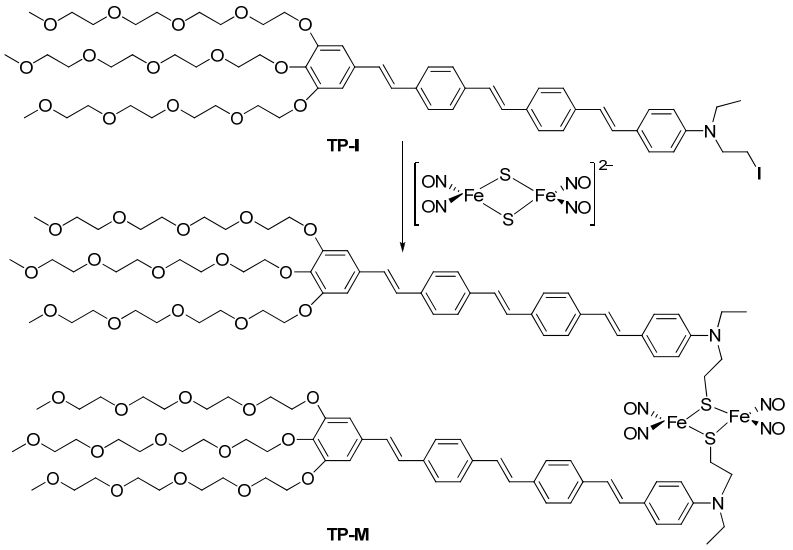

Scheme 2-1. Synthesis of the water soluble metal nitrosyl complex

We reported here the preparation of this water soluble metal nitrosyl complex with large TPA. We also report on its photochemical and photo-physical properties as well as its cellular cytotoxicity under one-, and two-photon excitation.

Linear absorption and emission

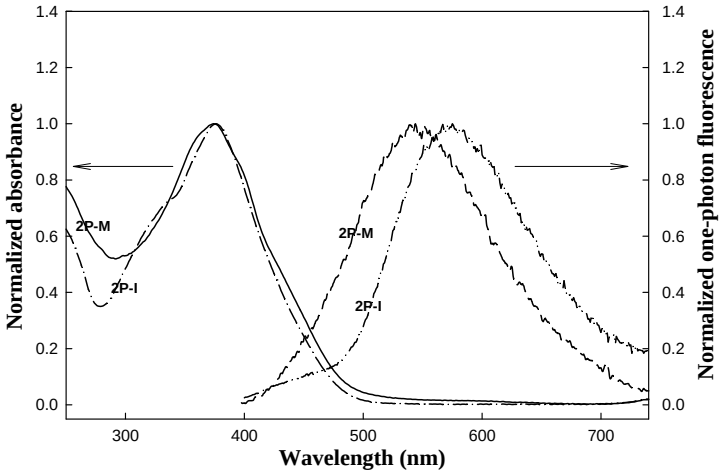

Fig. 2-2 Linear absorption and emission spectra for compounds **2P-I** and **2P-M**

As shown in Fig. 2-2, compound **2P-I** and compound **2P-M** have similar linear absorption spectrum. However, compound **2P-M** showed a hypsochromically shifted emission peak at 544 nm, compared to compound **2P-I** (λ_{em} = 575 nm). Table 2-1 summarizes their photophysical properties, including linear absorption maxima, molar extinction coefficients, emission maxima, and fluorescence quantum yields.

Two-photon absorption and emission

Shown in Fig. 2-3 is the fluorescence spectrum for compound **2P-I** excited at 775 nm. The energy of one photon with 775 nm wavelength is not high enough to excite a **2P-I** molecule from its ground state to the excited state; therefore more than one photons are needed for the excitation process. To further prove the nature of this process, the relationship between the fluorescence intensity and the laser intensity (775 nm, fs laser) was investigated. The results are shown in the inset of Fig. 2-3 where a log-log plot shows a slope of 1.92, demonstrating TPA. The two-photon excited fluorescence spectrum (in Fig. 2-3) is basically the same as its one photon excited fluorescence spectrum (in Fig.2-2), which confirms that both emissions are from the same excited state.

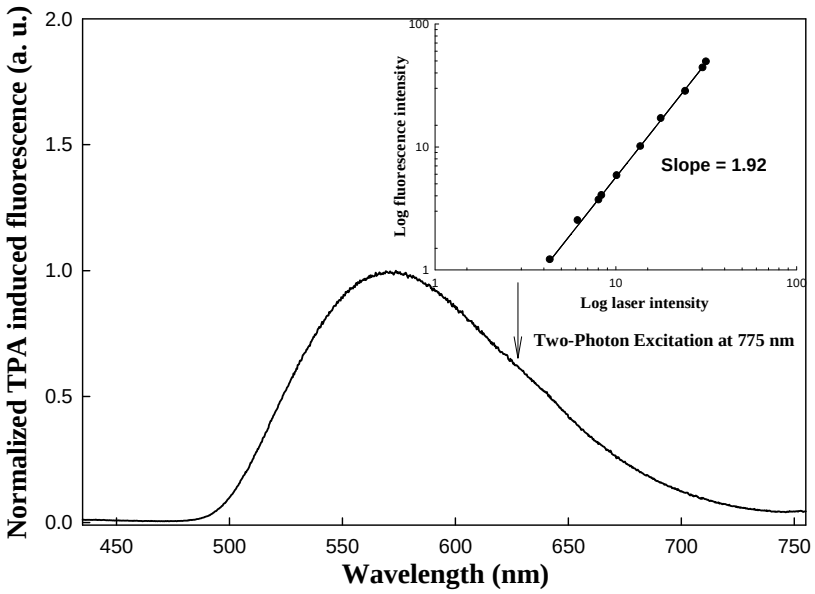

Fig. 2-3. Two-photon excited fluorescence for compound **2P-I** in water; (inset) fluorescence intensity versus the excitation laser intensity

To further optimize the excitation wavelength for two-photon excitation, TPA spectrum for compound **2P-I** was measured by using the two-photon excited fluorescence method, with Rhodamine 6G as a standard. The results are shown in Fig. 2-4, where one can see that compound **2P-I** has a TPA peak value of 660 GM at 740 nm. In addition to the measurement by the fluorescence method, the TPA cross section of **2P-I** at 775 nm was also determined by an independent absorption method (δ_{775} nm = 370 ± 55 GM) using a standard (AF350) with known . Both values for δ are in good agreement, considering the different nature of the methods employed for measurements. The fluorescence quantum yield for compound **2P-M** is quite low, which induces a large uncertainty in the measurement of TPA spectrum using the two-photon excited fluorescence method. Therefore, we measured its TPA properties using the nonlinear transmission method. As shown in Table 2-1, compound **2P-M** has a moderately large TPA cross section value of 682 GM at 775 nm, close to the value for compound **2P-I** (370 GM), considering compound **2P-M** has two TPA active structural units. These results reveal that when the two photon absorbing chromophore attaches to the Roussin's red salt ester, its two-photon absortivity is basically retained.

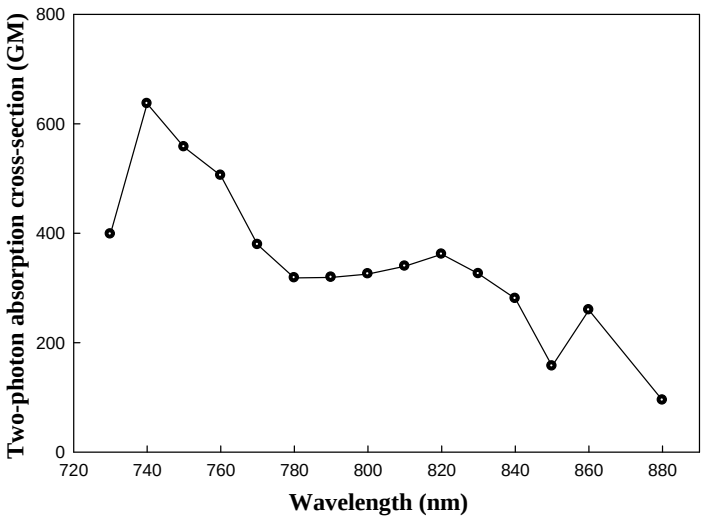

Fig. 2-4. Two-photon absorption spectrum for compound **2P-I** in water.

Photochemical properties

When the two-photon absorbing chromophore **2P-I** (antenna) is linked to Roussin's red salt ester (Fe-NO unit), there is an energy transfer from the antenna to the Fe-NO unit, which is responsible for the quenched emission found for compound **2P-M**. However, after light activation, the linkage between the antenna and the Fe-NO unit is disconnected (as shown in Fig. 2-1). Therefore, the pathway for the previous energy transfer disappears, and the resulting antenna chromophore exhibits a higher fluorescence quantum yield as usual. In other words, this NO releasing process is concomitant with increased fluorescence emission. We measured the one-photon excited fluorescence for compound **2P-M** (0.4 mM in H_2O) versus irradiation time of UV light, gradually increased emission was observed with increasing time of UV light irradiation. After 140 minutes of light irradiation, the fluorescence intensity was enhanced by a factor of 36. Light irradiation for an additional 10 minutes does not lead to a further increased in emission intensity. At this point when the solution was subjected to an EPR analysis, no signal was found, demonstrating the completion of the NO release process.

Similarly, an enhanced two-photon excited fluorescence should be also observed when compound **2P-M** is subjected to IR light irradiation. Fig. 2-5 shows the two-photon excited (775 nm) fluorescence spectra for compound **2P-M** before and after IR laser irradiation (775 nm). A 43-fold increased emission was observed after 110 minutes of IR light irradiation. Furthermore, we measure the peak intensity of two-photon excited fluorescence versus 775 nm laser irradiation time. The results are shown in the inset of Fig. 2-5, where one can see a monotonic growth of two-photon excited fluorescence in the beginning 110 minutes. However, after 110 minutes of light irradiation, the value of fluorescence intensity at 570 nm goes down due to possible photo-decomposition induced by intense laser.

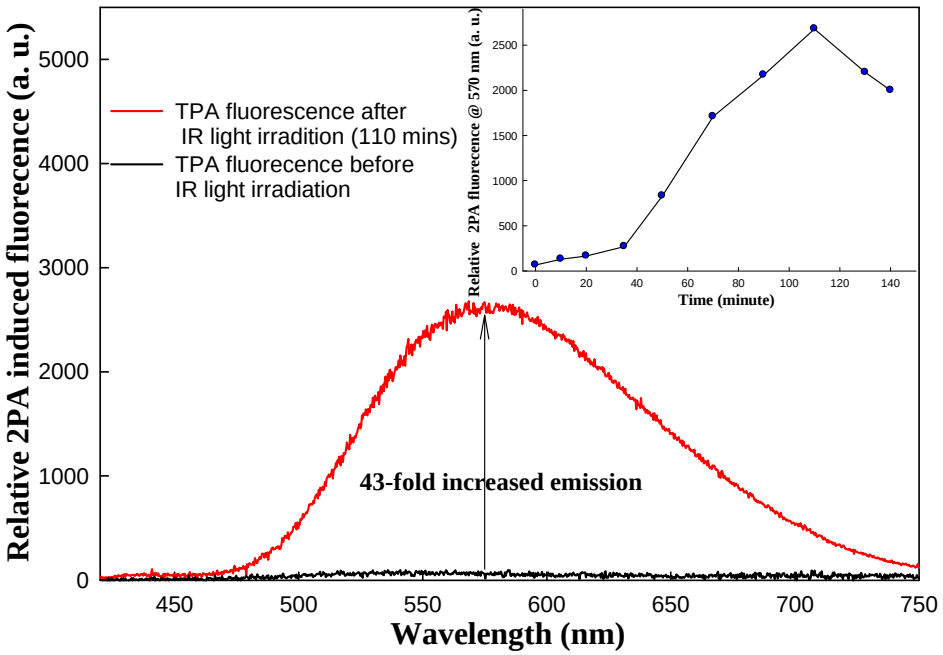

Fig. 2-5 Fluorescence spectra of compound **2P-M** (0.4 mM in H_2O) before and after 110-min IR laser irradiation; (inset) fluorescence intensity at 570 nm versus irradiation time of 775 nm laser light.

III. Backward stimulated scattering enhanced optical limiting in multi-photon active $CdTe_xSe_{1-x}$ quantum dots system

In this work, we present the properties of backward SBgS from a multi-photon absorbing quantum dots system, and demonstrate the enhanced optical limiting behavior of this system based on both SBgS and MPA, working at three different laser wavelengths and in ns-regime.

The nonlinear medium utilized for this study is the $CdTe_xSe_{1-x}$ (x=0.25) quantum dots (QDs) homogeneously suspended in chloroform ($CHCl_3$). In our case this type of sample medium can be of double functions: it acts as a nonlinear scattering medium to generate backward stimulated scattering, while it is also a nonlinear absorbing medium exhibiting MPA capability. The $CdTe_xSe_{1-x}$ QDs was prepared using hot colloidal synthesis method. Briefly, Se and Te mixture with molar ratio of 75:25 was prepared in trioctyl phosphine (TOP) solution in advance. Separately, 4 mmol of cadmium oxide was dissolved in 8 g of trioctyl phosphine oxide (TOPO) and 4 g of myristic acid. The mixture was heated at ~290^{o}C for 35 minutes under argon flow, then 1 mL TOP:Se:Te solution was injected under vigorous stirring into the hot reaction mixture. After the injection, the reaction temperature was decreased and held at 230^{o}C and stirred for ~15-20 minutes. The nanocrystals (NCs) were separated from the surfactant solution by addition of ethanol and centrifugation. The dark-brown NC precipitate could be redispersed in various organic solvents including hexane, toluene, and chloroform. The TEM microphotograph of these quantum dots is shown in the inset of Fig. 3-1, from which we know the average QD-size was about 5-7 nm.

The linear transmission spectra of the 1-cm long pure solvent ($CHCl_3$) sample and four $CdTe_xSe_{1-x}$ QDs/$CHCl_3$ samples with different concentration are shown in Fig. 3-1. In this figure, we see that there is a strong UV absorption band with a rapidly decaying tail covers whole visible spectral range and basically stops around 800-nm wavelength position. For the three most commonly used pulsed laser wavelengths, i.e. 532 nm, ~800 nm and 1064 nm, one can expect that the multi-photon absorption may take place at these wavelengths, because the two- or three-photon energy of these excitation wavelengths falls into these UV absorption band.

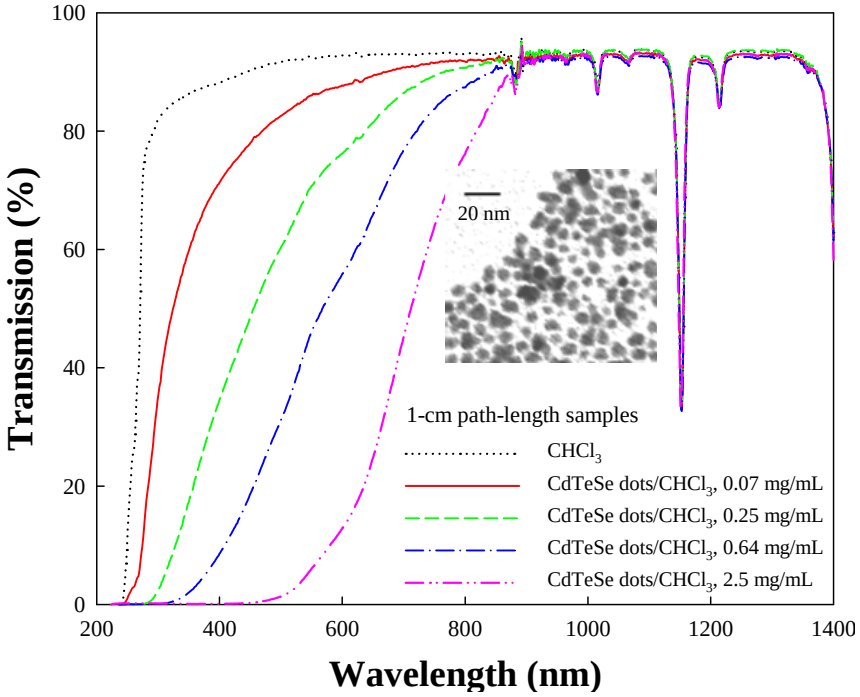

Fig. 3-1 Linear transmission spectra of the pure solvent ($CHCl_3$) and three CdTeSe QDs/$CHCl_3$ samples with different concentrations. The TEM image of CdTeSe QDs is shown in the inset.

In our experiment, as schematically shown in Fig. 3-2, three laser beams of different wavelengths (532, 816 and 1064 nm) were separately utilized to generate backward stimulated Bragg scattering in 1-cm long $CdTe_xSe_{1-x}$ QDs/$CHCl_3$ samples with different concentrations. The pump beam was focused via an f=15-cm lens onto the center of a given sample cuvette of 1-cm path-length. To avoid the reflection influence from the optical windows of the cuvette, the incident angle of the pump beam was $\geq$ (5˚-8˚). As the pump beam was linearly polarized, the input pump energy can be varied by rotating a polarized prism.

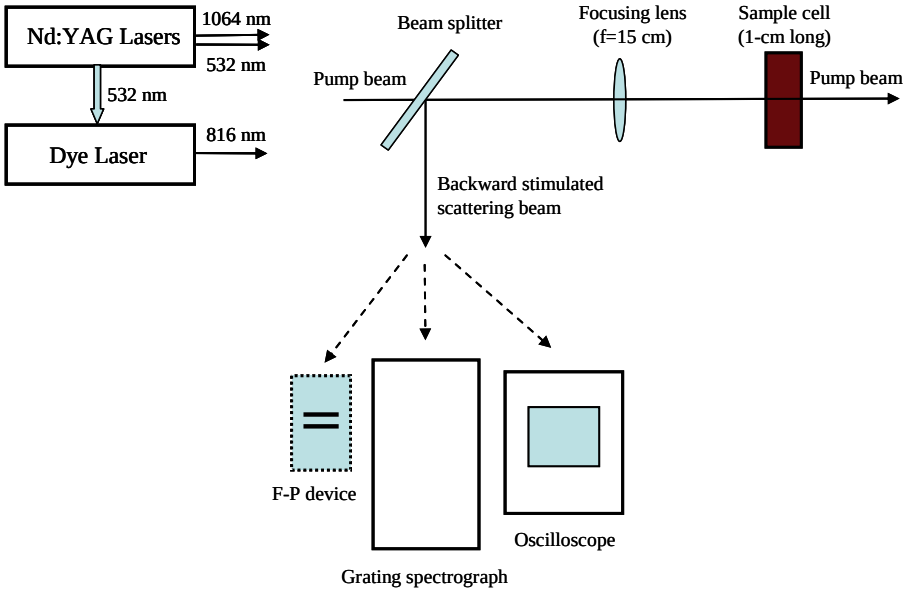

Fig. 3-2 Experimental setup for generating backward stimulated scattering and optical limiting measurements.

It is found that once the input pump energy is higher than a certain threshold value for a given sample solution, a highly directional backward stimulated Bragg scattering (SBgS) featuring no frequency-shift can be readily observed through the reflection from a beam splitter. Table 3-1 summarizes the pump threshold values (in both energy and intensity) for three QDs/$CHCl_3$ samples and the pure solvent ($CHCl_3$) sample of the same 1-cm path-length, measured at three different pump wavelengths. From this table, one can see that the threshold values for generating SBgS in the QDs/$CHCl_3$ samples can be 5-30 times lower than that for generating SBS in a pure solvent sample. To estimate the local pump intensity levels in the sample medium, we have to assume the average spot size (radius w_0) of the focused pump beam over its Rayleigh (focal depth) range. Based on the divergence angle and the focal length, we estimated $w_0 \approx 42$ μm for 532-nm and 1064-nm laser beams, and $w_0 \approx 50$ μm for 800-nm laser beam.

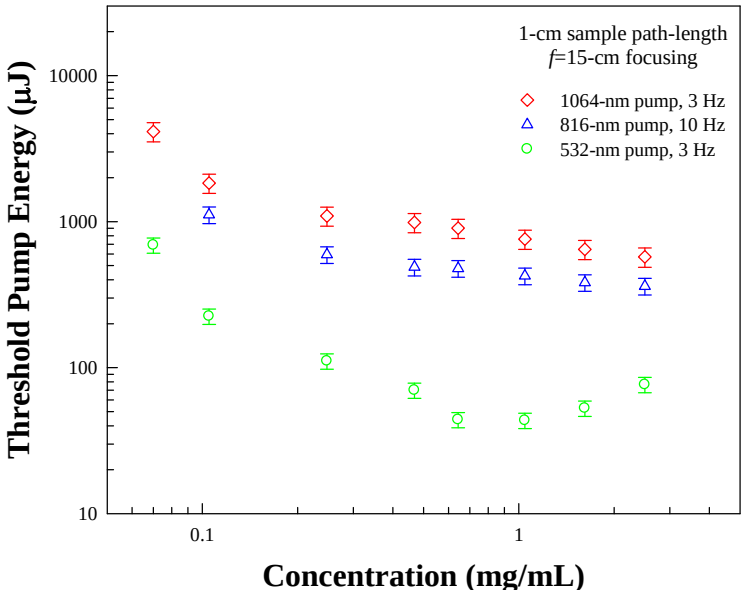

Fig. 3-3 Measured threshold energy values as a function of sample concentrations by using three pump wavelengths.

The measured values of output pulse energy of backward SBgS as a function of the input pump energy are presented in Fig. 3-4 for three samples excited by different pump wavelengths. The results from a 0.25 mg/mL sample solution pumped by 532 nm laser pulses indicat an ~14% energy transfer efficiency from the pump beam to the backward stimulated scattering beam, this value is also defined as nonlinear reflectivity of the backward stimulated generation. The results from other two samples pumped by 816-nm and 1064-nm laser pulses showed ~14% efficiency for 816-nm pump and ~8.3% for 1064-nm pump case, respectively.

It is known that semiconductor QDs suspended in certain solvents manifest multi-photon absorption (MPA) capability in suitable wavelength ranges. Both MPA and backward SBgS are intensity-dependent nonlinear processes; they can be combined to realize an enhanced optical power limiting performance. To demonstrate this feasibility, we measured the nonlinear transmission of 1-cm samples as a function of the input pulse energy (or intensity), and also measured the nonlinear reflectivity of the backward SBgS versus the input pump energy. For 532-nm pumped sample of 0.25 mg/mL concentration, the measured nonlinear transmission values versus the input pump energy values are presented in Fig, 3-4(a), and the nonlinear reflectivity data are shown in Fig. 3-4(b). It should be pointed that the measured nonlinear transmission data could not be fitted by either MPA mechanism or SBgS mechanism alone. However, these experimental data can be well fitted if we write the nonlinear transmission as

$$T'(I_p) = T_{2PA}(I_p) - R(I_p), \tag{3-1}$$

where I_p is the input pump intensity (in GW/cm^2), $R(I_p)$ is the measured nonlinear reflectivity of SBgS, and $T_{2PA}(I_p)$ is the nonlinear transmissivity due to two-photon absorption (2PA) expressed by

$$T_{2PA}(I_p) = T_0 \frac{\ln(1+\beta I_p l_0)}{\beta I_p l_0}. \tag{3-2}$$

Here β is the 2PA coefficient for a given medium; T_0 is the linear transmission at the pump wavelength. In Fig. 3-4 (a), the doted-line is the pure 2PA fitting curve while the solid-line is the best fitting curve given by Eqs. (3-1) & (3-2) with the fit parameter of β=2 cm/GW. The results shown in Fig. 3-4(a) reveal two facts: (i) when the input pump intensity is lower than the threshold value, the nonlinear attenuation is only determined by 2PA; (ii) when the input pump intensity is much higher than the threshold value, a considerable part (~14%) of the pump energy is transferred to the backward stimulated scattering. These two combined facts lead to a deeper drop of nonlinear transmission following the increase in input intensity and provide an enhanced optical limiting performance. Considering that the two-photon energy of 532-nm radiation just falls in the strong UV absorption band of the sample medium, it is not surprised that the 2PA plays the major nonlinear absorption role in this case.

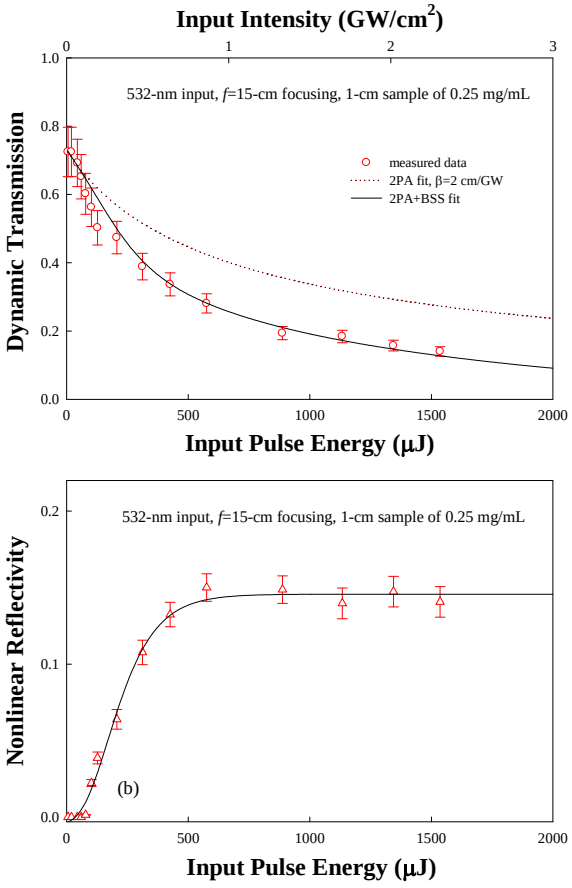

Fig. 3-4 Measured (a) nonlinear transmission and (b) nonlinear reflectivity of the sample pumped by 532-nm laser pulses. In (a) the dotted-line curve is a 2PA fitting curve, the solid-line is the fitting curve by considering both 2PA and backward stimulated scattering (BSS).

IV. Optical limiting, stabilization and reshaping of laser pulse series passing through a nonlinearly absorbing polymer rod

In recent years, researchers are more interested in developing various two-photon absorbing materials for applications. Based on their property of intensity dependent nonlinear transmissivity, these materials can be successfully utilized for optical limiting, optical stabilization and reshaping. Since the probability of two-photon absorption (2PA) at a given position within a sample medium is proportional to the square of the local intensity of the input excitation light, a higher spatial resolution of the nonlinear interaction between the excitation beam and the nonlinear medium can be expected along both transverse and longitudinal directions of a focused excitation beam. Taking this advantage researcher can realize frequency-up-converted three-dimensional (3D) imaging and microscopy, 3D optical data storage, and 3D optical micro-fabrication. Up to date, most reported organic two-photon absorbing materials are based on various novel chromophore molecular systems and the nonlinear optical characterization is usually conducted in their solution phase. From the view-point of applications, two-photon active chromophore doped polymer films, waveguides and rods are more promising for various application purposes. In this Letter, we report a novel chromophore (AF289) doped polystyrene rod as a highly two-photon absorbing medium for nonlinear optical performances, and compare it with the AF289 solution in tetrahydrofuran (THF).

The chromophore AF350 is synthesized in Air Force Research Laboratory and its molecular structure is shown in the inset of Fig. 4-1. The best way to make a chromophore-doped polymer rod is to dissolve the chromophore in a chosen liquid monomer, and then to polymerize the solution in a certain temperature range. We have tried three different monomers (MMA, HEMA, and styrene) and found that the last one manifests a higher solubility for AF289, and can be employed for making a good quality rod after polymerization. To prepare the two-photon absorbing rod used for our nonlinear optical experiment, we dissolved 20-mg AF289 in a 1-mL liquid monomer (styrene) of polystyrene and added 5-mg benzoyl peroxide as an initiator. Such prepared AF289-monomer solution was put in an oven for polymerization at ~70 ºC for ~72 hours. After polymerization we could get AF289 doped polystyrene rod of high optical quality with a concentration value of 0.017 M/L. To measure the linear absorption spectrum, such prepared doped rod sample is too thick. Therefore, a doped polymer film was prepared by dissolving a small cut piece of the doped rod into chlorobenzene, and then spin-coated the polymer solution on a quartz plate.

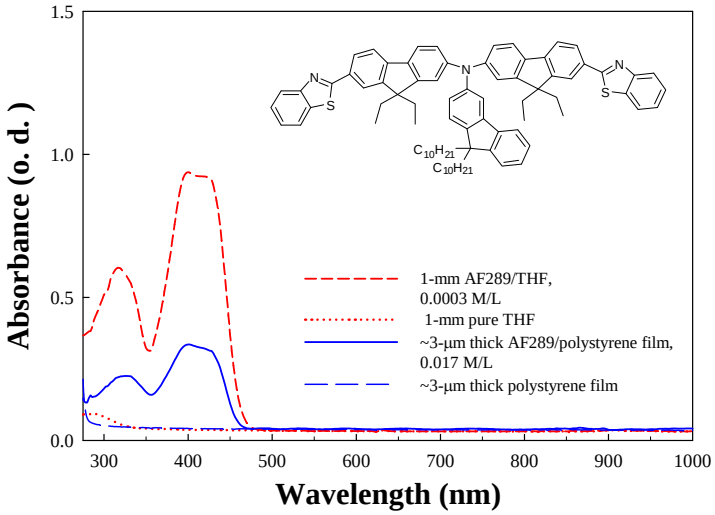

Fig. 4-1 Linear absorption spectra of 1-mm AF289/THF sample (short-dashed line), 1-mm THF sample (dotted line), ~3-μm AF289/polystyrene film (solid line), and ~3-μm polystyrene film (long-dashed line).

Shown in Fig. 4-1 are the measured linear absorption spectra of a 1-mm AF289/THF solution (short-dashed line), 1-mm pure THF sample (dotted line), ~3-μm AF289/polystyrene film (solid line), and ~3-μm undoped polystyrene film sample (long-dashed line), respectively. In Fig. 4-1 one can see that the relative absorption spectral curves of the AF289 doped film and AF289/THF solution are quite similar: the strongest band is located around 400-nm wavelength position, and second band located around 320-nm position. For the doped film sample the peak ratio of these two bands is ~3.1, whereas for the solution sample this ratio is ~2.9. Another difference is that the peak wavelength position of the second band for the doped film sample is somewhat blue-shifted. Since the main absorption band for AF289 is located around 400 nm position, one may expect that the two-photon absorption should take place with the excitation wavelength around 800 nm.

For nonlinear optical measurements, the two-photon excitation source was a Ti:Sapphire laser oscillator/amplifier system (CPA-2010 from Clark-MXR) that provided laser pulses of ~775-nm wavelength, ~160-fs pulse duration, ~3-mm beam diameter, and 1-kHz repetition rate.

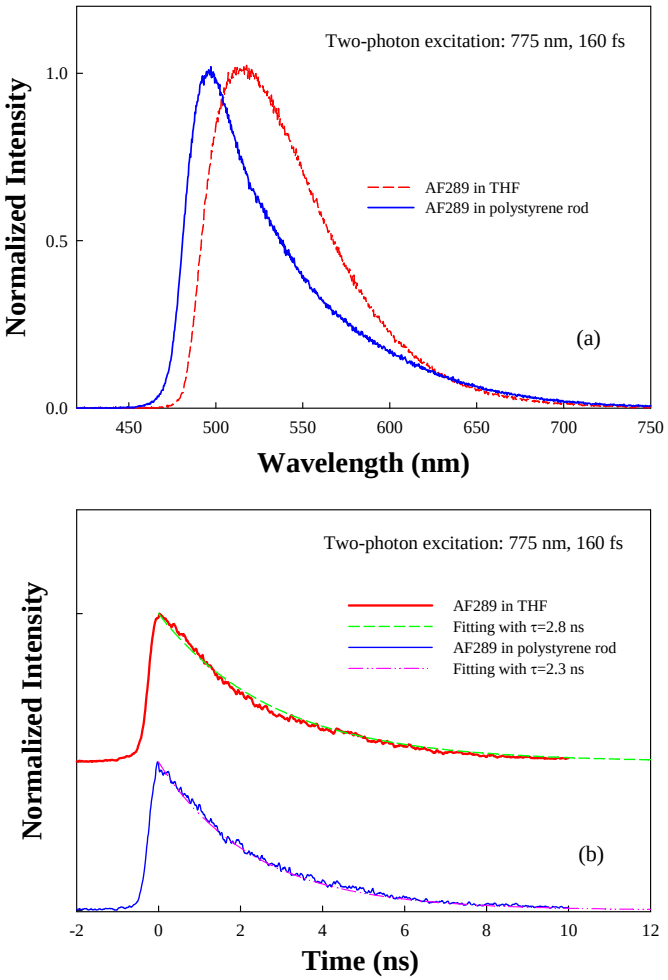

Fig. 4-2 Two-photon excited fluorescent spectra (a) and decay curves (b) of AF289 in THF and AF289 in polystyrene, respectively.

Upon the excitation of these laser pulses, both AF289 doped rod and solution sample manifest strong two-photon induced fluorescent emission. Shown in Fig. 4-2(a) are the measured frequency upconverted emission spectra from a doped rod sample and a solution sample by using a grating spectrometer, in which one can see that the two-photon excitation induced emission spectral curve is narrower and blue-shifted in comparison to the curve of the solution sample. In this case, both samples have the same concentration value (0.017 m/L) and to avoid the re-absorption effect of the emission signals propagating inside the sample medium, the curves shown in Fig. 4-2(a) are recorded only by those signals emitted from a shallow surface layer of the tested samples. Shown in Fig. 4-2(b) are the two-photon induced fluorescent decay curves of the two samples measured by a streak camera system (C-5680-22 from Hamamatsu), these two measured decay curves can be well fitted with two single exponential curves with different decay constant. The best fitting lifetimes for the doped rod sample and the solution sample are 2.3 ns and 2.8 ns, respectively.

In nonlinear transmission measurement, the laser beam was focused by an *f*=20-cm lens on the center of the 1-cm path-length doped rod sample or solution sample. Moreover, to avoid the possible thermal lensing effect, the incident laser beam was also passed through a rotating chopper possessing a ratio of opening/blocking ratio of 1:10, so that the average input pulse number per second was reduced by a factor of 10.

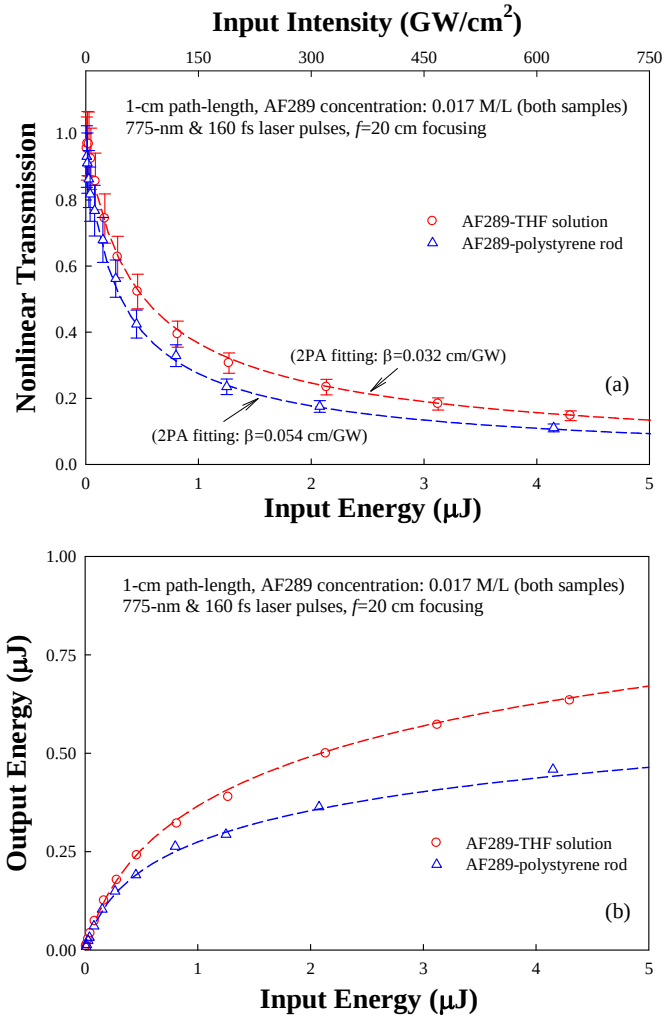

Fig. 4-3 (a) Nonlinear transmission as a function of the input pulse energy (intensity); (b) Output/input characteristic curves for two compared samples.

Shown in Fig. 4-3(a) are the measured data of nonlinear transmissivity as a function of the input pulse energy and the intensity. The best fitting parameters is β=0.032 cm/GW for the solution sample and β=0.054 cm/GW for the doped rod sample; the corresponding 2PA cross-section (σ_2) values for these two samples are 0.31×10^{-20} cm^4/GW and 0.53×10^{-20} cm^4/GW, respectively. The uncertainty of such estimated β and σ_2 values are mainly determined by the uncertainty of estimating the input intensity inside the tested medium and should be around ±20%. The measured output pulse energy values versus the input energy are shown in Fig. 4-3(b), in which the two dashed lines represent the theoretical fitting curves with the corresponding β values given above. Figure 4-3(a) & (b) demonstrate typical 2PA-based optical power limiting

effect, and at the 775-nm input wavelength, the AF289 doped polystyrene rod exhibits a higher 2PA coefficient and therefore better optical limiting performance.

The unique feature shown in Fig. 4-3(b) is that at high input levels a considerable large input pulse fluctuation only leads to a much smaller output fluctuation. This is the basis of utilizing 2PA for optical stabilization application. As an experimental example, shown in Fig. 4-4 are the peak intensity traces for the input pulses (a) and the output pulses (b) passed through the AF289 doped polymer rod. These traces are recorded by a two-channel 500-MHz digital oscilloscope (Infinum from Hewlett-Packard), working in its "peak detect" mode. The average input pulse energy (intensity) is ~2 μJ (~300 GW/cm^2) and the other experimental conditions are the same as mentioned before. In Fig. 4-4(a) & (b), both traces of the input and output pulses are normalized to their average maximum levels. The peak intensity fluctuation of the input pulses is $\Delta \approx \pm 10$ %, while the fluctuation of the output pulses is only $\Delta \approx \pm 3.3$ %. The 3-fold reduction of the output pulse fluctuation is the evidence of the function for optical stabilization.

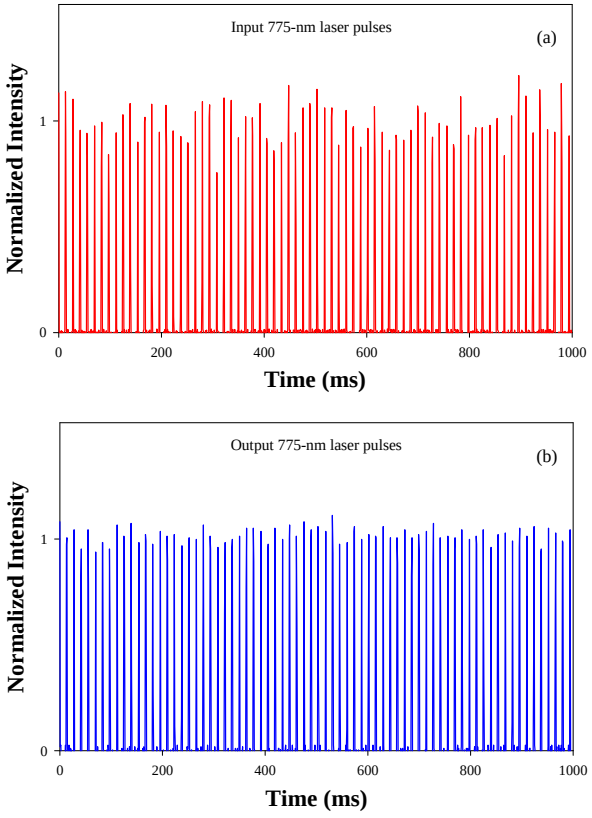

Fig. 4-4 Optical stabilization effect demonstrated by the fluctuations of the normalized input pulses (a) and the normalized output laser pulses (b).

The same nonlinear transmission property of a two-photon absorbing medium can also be utilized for reshaping the temporal profiles of laser pulse series with different initial peak intensity ratio. Shown in Fig. 4-5(a) are the input pulse traces that manifest two groups (A & B) of laser pulses. Group-A pulses are passed through the fully open holes of a rotating chopper, whereas group-B pulses are passed through the other open holes attached with an attenuation

polymer film. At the average input energy level for A-pulses is ~1.5 μJ, the measured average intensity ratio between the input pulse group-A and group-B is $\frac{I_A}{I_B} \approx (4 \sim 5)$. Figure 4-5(b) shows the corresponding traces of the output pulses after passing through the same 1-cm AF289 doped polymer rod. In the latter case, one can see that for the output laser pulses, the intensity ratio between these two groups is changed to $\frac{I_A}{I_B} \approx (2.5 \sim 3)$. So that the relative pulse profiles of these two group of pulse series can be reshaped.

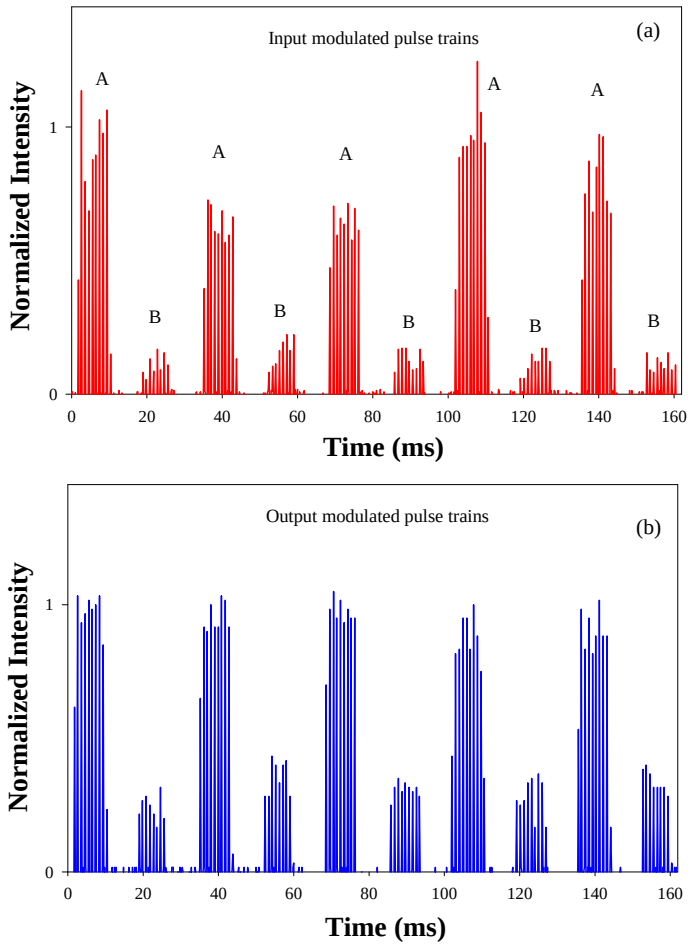

Fig. 4-5 Temporal reshaping effect demonstrated by the profiles of the normalized input pulses (a) and the normalized output laser pulses (b).

V. Highly photosensitive PbS nanoparticles functionalized with short-chain ligands, designed for enhancement of photorefractive effect at communication wavelength (1.34 mm)

Investigations on Photorefractive (PR) effect carried out in this reporting periods were mainly focused on the issues related to the optimization of photosensitivity in hybrid nano-composites containing lead sulfide (PbS) nanoparticles (NPs) with optical activity in near-infrared (NIR) spectral range. To improve the optoelectronic properties, we have applied a ligand de-protection strategy to demonstrate a relative improvement in the efficiency of a charge generation of hybrid PR composites for PR applications. The resulting shortened ligands on NCs lead to enhancement of both photocurrent and diffraction efficiency in corresponding film devices. As a result, the photon generation quantum efficiency in photoconductivity study was improved to be over 20%, and the two-beam coupling (TBC) gain coefficient was pronounced as 173 cm^{-1}.

Photoconductivity results

Efficient charge generation and transporting at the operation wavelength are required for buildup of large internal electric field. Therefore, the photoconductivity and photosensitivity were investigated as a function of applied electric field excited at 1.34 μm. As shown in Fig. 5-1 (a), the current-voltage relationship (I-V) was measured in dark and different input laser power. As a result, the photocurrent increased from $2*10^{-6}$ (A) in dark to $7.5*10^{-5}$ (A) at 18 mW excitation power when the applied electric field was 100 V/μm. The I-V curves were nonlinear behavior. In order to choose the best NPs concentration for photorefractive effect, the dependence of photoconductivity and charge-generation quantum efficiency on PbS NPs concentration were studied and shown in Fig. 5-1(b) & (c), respectively. Quantum efficiency (Φ) is an important parameter to describe the charge-generation property of the material, which can be determined using the equation:

$$\Phi = \frac{N_{cc}}{N_{ph}} = \frac{J_{ph}/e}{I\alpha d/h\nu} = \frac{J_{ph}hc}{I\lambda e\alpha d} \qquad (5\text{-}1)$$

where N_{cc} is the number of charge carriers generated per unit volume, N_{ph} is the number of photons absorbed per unit volume, J_{ph} the photocurrent density, e fundamental unit charge, I the illumination intensity of the beam, α the absorption coefficient of the sample, d the sample thickness, h the Plank's constant, ν the frequency of incident light beam, c the speed of light, and λ the wavelength of light beam. Compared with our previous work, the quantum efficiency of short ligand functionalized PbS NPs was observed to exhibit as high as 20%, which is three times larger than the value of long ligand PbS NPs.

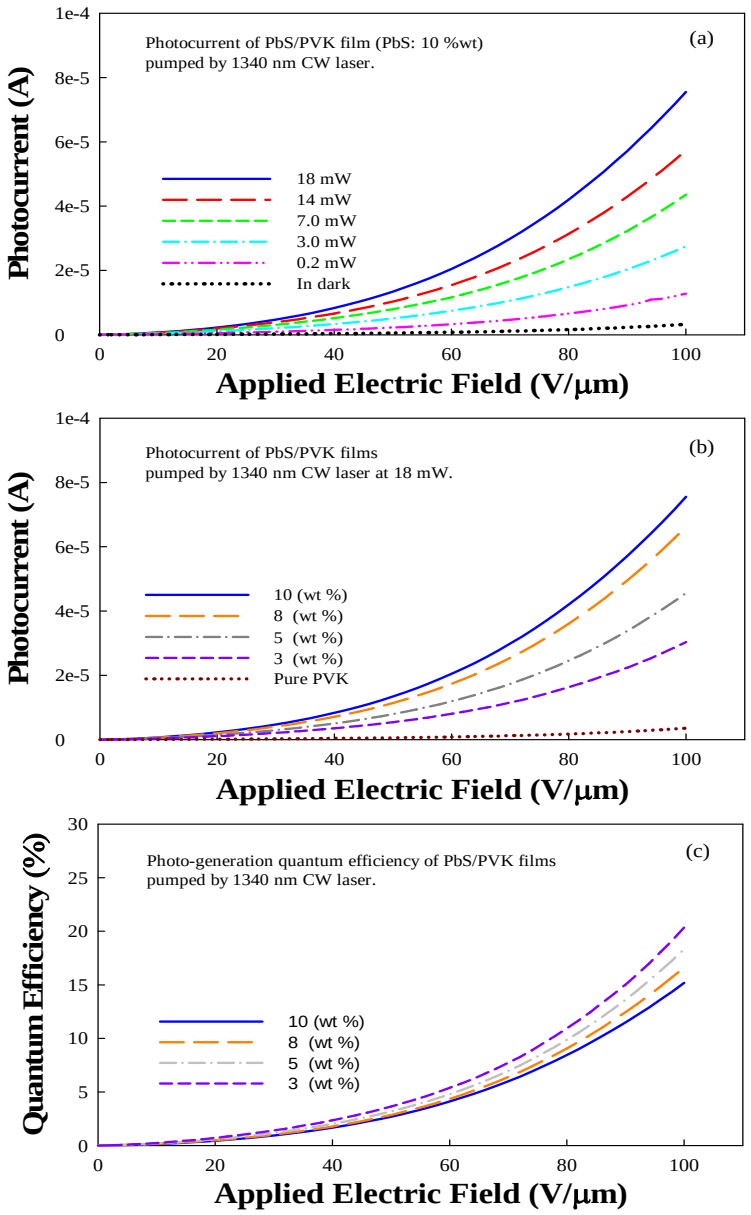

Fig. 5-1 Dark current and photocurrent as a function of applied electric field for PVK: PbS-QD composites pumped by different input laser power (a); Photocurrent (b) and photo-generation quantum efficiency (c) versus applied electric field for the composites containing various amounts (wt %) of PbS-QDs.

From Fig. 5-1(c), it could also be concluded that the best concentration of PbS NPs for highest quantum efficiency is 3% weight percent, which is because of the dependence of charge mobility μ on the average distance of nanoparticles ρ derived from the concentration: $\mu \propto \rho^2 e^{-2\rho/\rho_0}$, ρ is the localization radius.

Two-beam Coupling

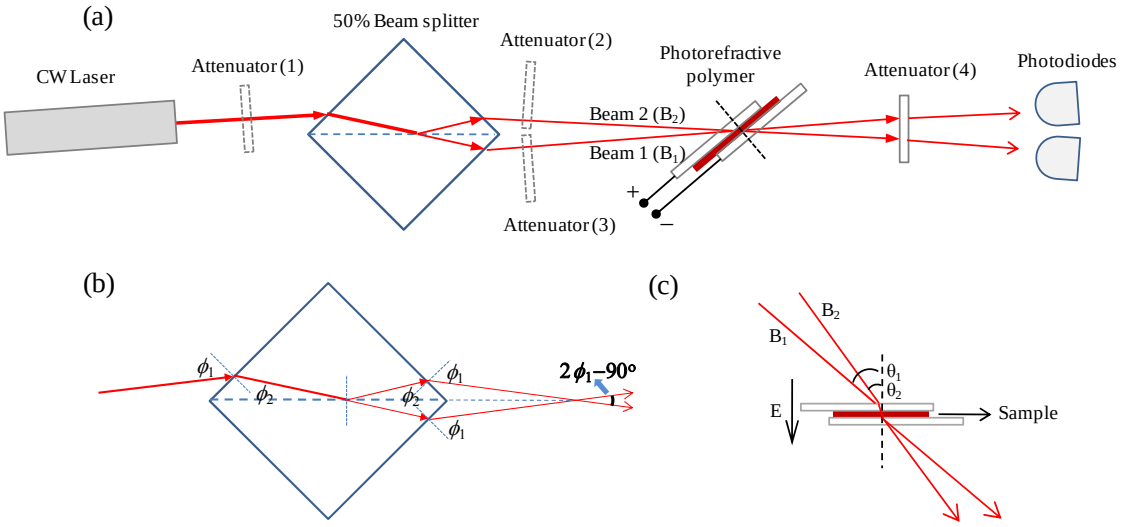

Fig. 5-2 (a) Experimental setup for two beam coupling; (b) A 50% beam splitter worked as a beam coupler; (c) Beam geometry and applied electric field (E) direction in this report; The incident angles of beam-1 and beam-2 with the sample normal are θ_1 and θ_2, respectively.

The unique feature of PR effect was described as a phase shift between the refractive index grating and the interference pattern, which could be confirmed by the asymmetric energy transfer in the two-beam coupling (TBC) experiment. The experiment setup was shown in Fig. 5-2(a). In the previous setup, the two beams were reflected by two infrared (IR) mirrors before passing through the sample. In our experiment, we unexpected found that two beams could meet again after leaving the beam splitter if the incident beam is at an appropriate angle. In Fig. 5-2 (b), we demonstrated the light path of the beam transmission. It could be proven that the angle between the two output beams is ($2\phi_1$-90^o), in which, ϕ_1 is the incident beam angle. Besides that, identical passing length of the two beams could be automatically matched. We will benefit from replacing the two mirrors by one beam splitter, because there is no need to adjust too much when we change the angle between two beams due to automatic light-pass length identity. Beam geometrical arrangement in all our studies in this paper was shown in Fig. 5-2(c), the incident angle of Beam 1 and Beam 2 are θ_1 and θ_2, respectively. The direction of applied external electric field was also directed as shown in the figure. In this case, the energy was evidently transferred from Beam 2 to Beam 1.

Prior to the two-beam coupling, the absorption of films were measured by using UV-absorption-IR spectrometer. In Fig. 5-3, one could find that the absorption from the PbS NPs based on quantum confinement was preserved in the polymer matrix. Chloroform was chosen to dissolve the mixture in order to keep the NPs from aggregating because of its fast volatility. The absorbing coefficient of sample in this study is 15 cm^{-1}.

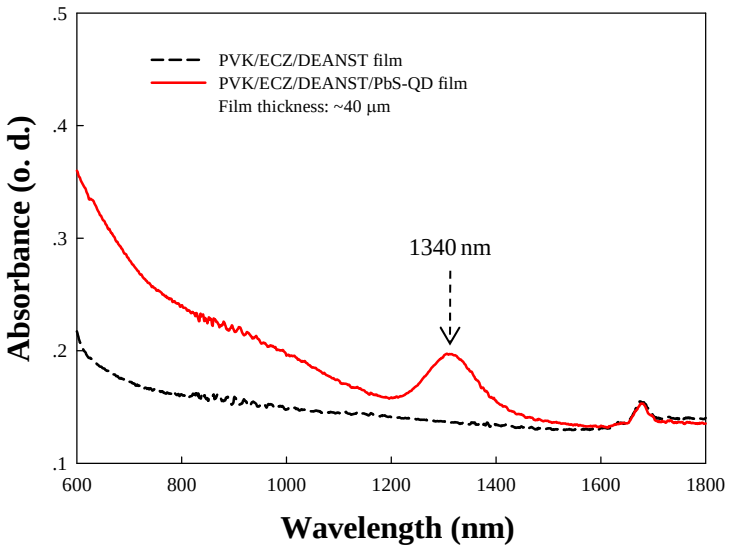

Fig. 5-3 Absorption spectra of PVK/ECZ/DEANST (50:30:20 in weight) film (dashed line) and PVK/ECZ/DEANST (48:30:20:2 in weight) film (solid line) with thickness of ~40 μm.

Two-beam coupling experiment were taken according to the setup and arrangement shown in Fig. 5-2, and excited by a 632.8 nm He-Ne laser. As well known, the experimental conditions such as input beam ratio were crucial issue affecting the TBC gain efficiency (η), which was defined as equation: $\eta = \Delta E / E_{B_1}$, where ΔE is transferred energy, and E_{B_1} is the input energy of Beam 1. Three ways were applied by changing the input energy of Beam 1 or Beam 2 independently as well as adjusting them together with a fixed beam ratio. The initial input power of Beam 1 and Beam 2 were 0.32 mW and 0.86 mW respectively, and they were decreased by passing through the neutral attenuators.

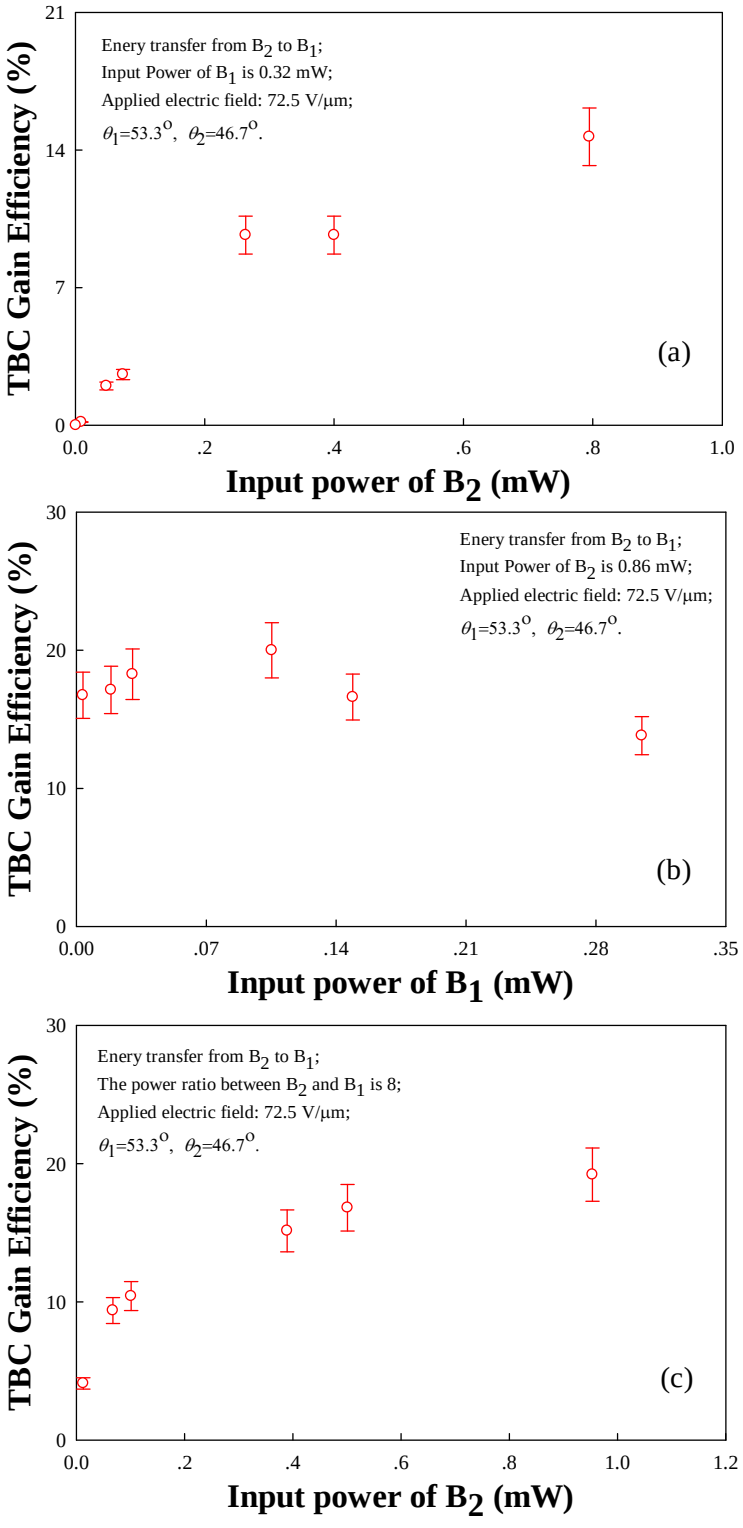

Fig. 5-4 Two-beam coupling (TBC) gain efficiency (η), defined as $\eta=\Delta E/E_{B1}$, related to different input power of beam-1 and beam-2, which were changed separately (a and b) and together with a fixed power ratio (c). ΔE is transferred energy, and E_{B1} is the input energy of Beam 1.

As shown in Fig. 5-4, three major things could be mentioned: (i) gain efficiency increased first rapidly then slowly, when increasing the power of Beam 2; (ii) gain efficiency was first increasing then decreasing with the power of Beam 1 increasing; (iii) gain efficiency increased as the power of Beam 1 and Beam 2 both increased. These phenomenon could be explained by considering that the transferred energy were dependent on three parameters: input power of Beam 1, input power of Beam 2 and reflection of the refractive index grating, which was monitored by modulation depth of the interference pattern grating. Therefore, we could find that the deepest modulation depth was forming at 1:1 beam ratio, while the largest gain efficiency was received at 1:8 beam ratio (Beam 1: Beam 2).

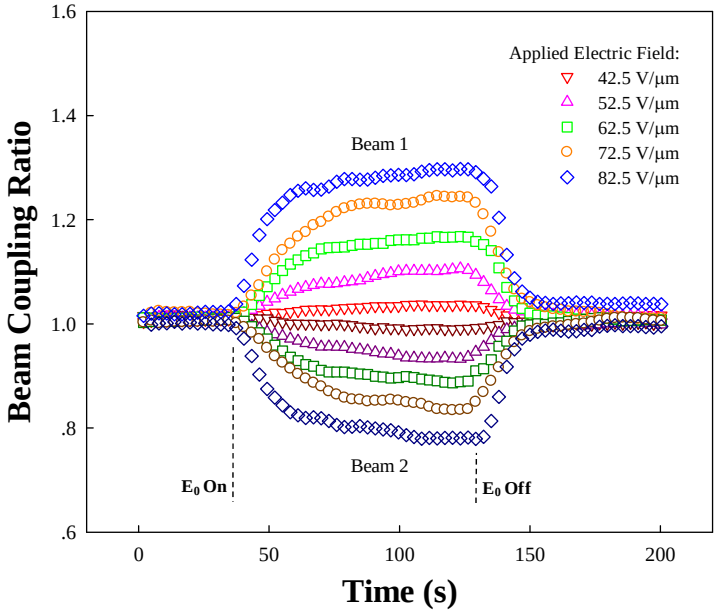

Fig. 5-5 Energy exchange ratio between two beams (Beam 1: Beam 2=1:8 in ratio) in the TBC experiments of PVK: ECZ: DEANST: PbS-QD composites with time, for a range of applied electric field. The external electric field was turned on at *t*= 35 s and turned off at *t*= 130s.

As the optimized experimental conditions, beam ratio and two incident angles were selected at 1:8, θ1=53.3º and θ2=46.7º for TBC experiments. The signals of two beams were detected by photodiodes and recorded by boxcar with respect to time. The applied electric field was turned on at t= 35 s and turned off at t= 130s. The typical experimental measurement verifying effective energy exchange between laser beams is illustrated in Fig. 5-5. As a result, the raising time of Beam 1 was about 20 s, while the falling time was a little bit faster around 10 s, which could be understand that there was two steps for the raising process: charge generation and transport and reorientation of nonlinear optical molecules, while the falling process was established by the latter one.

The TBC gain coefficient Γ is given in the term of the experimentally determined γ_0 and β, as

$$\Gamma = \frac{\cos\theta}{d}\left[\ln(\gamma_0\beta) - \ln(\beta + 1 - \gamma_0)\right], \quad (5\text{-}2)$$

where d is the sample thickness, β is the input beam ratio and $\gamma_0 = P_1/P_0$, P_1 being the intensity of the signal (Beam 1) with pump (Beam 2), P_0 being the intensity without pump. A maximum TBC gain coefficient of 173 cm^{-1} at an applied electric field of 82.5 V/μm was observed. For a practical point of view, the optical amplification, Γ, needs to exceed the optical loss, α, of the PR sample. In the present case, the net gain coefficient Γ-α was 158 cm^{-1} at 82.5V/μm.

Conclusions

The PR composite based on short-chain-ligands functionalized PbS NPs were demonstrated to have strong photocurrent and good performance of PR effect by photoconductivity and TBC experiments. The resulting quantum efficiency was improved to be over 20% at applied field of 100 V/μm, which was three times higher than the value for PbS NPs coved with long-chain ligands, like oleic acid. Furthermore, the TBC gain coefficient in this study is about 173 cm^{-1} at applied electric field of 82.5 V/μm, which is one of the highest reporting values to our knowledge. Therefore, PbS Nps functionalized with short-chain ligands has potential applications in the charge generation devices such as PR.

Publications

1. G. S. He, Q. Zheng, K.-T. Yong, A.I. Ryasnyanskiy, P.N. Prasad, and A. Urbas, Two-photon absorption based optical limiting and stabilization by using a CdTe quantum dots solution excited at optical communication wavelength of ~1300 nm," *Appl. Phys. Lett*. **90**, 181108 (2007).

2. G. S. He, K.-T. Yong, Q. Zheng, Y. Sahoo, A. Baev, A. I. Ryasnyanskiy, and P. N. Prasad, "Multi-photon excitation properties of CdSe quantum dots solutions and optical limiting behavior in infrared range," *Optics Express* **15**, 12818 (2007).

3. G. S. He, Q. Zheng, and P. N. Prasad, "Stimulated Rayleigh-Bragg scattering in a three-photon absorbing medium and its phase-conjugation property," *J. Opt. Soc. Am. B* **24**, 1166 (2007).

4. G. S. He, Q. Zheng, A. Baev, and P. N. Prasad, "Saturation of multiphoton absorption upon strong and ultrafast infrared laser excitation," *J. Appl. Phys*. **101**, 083108, 2007.

5. A. Baev, M. Samoc, P. N. Prasad, M. Krykunov, and J. Autschbach, "A Quantum Chemical Approach to the Design of Chiral Negative Index Materials", *Opt. Express* **15,** 5730-5741 (2007).

6. S. Jockusch, Q. Zheng, G. S. He, H. E. Pudavar, D. J. Yee, V. Balsanek, M. Halim, D. Sames, P. N. Prasad, and N. J. Turro, "Two-Photon Excitation of Fluorogenic Probes for Redox Metabolism: Dramatic Enhancement of Optical Contrast Ratio by Two-Photon Excitation," *J. Phys. Chem. C* **111**, 8872 (2007).

7. I. I. Smalyukh, D. S. Kaputa1, A. V. Kachynski1, A. N. Kuzmin1, and P. N. Prasad1, "Optical trapping of director structures and defects in liquid crystals using laser tweezers,",

Opt. Express. **15**, 4359-4371 (2007).

8. A. V. Kachynski, A. N. Kuzmin, and P. N. Prasad, I. I. Smalyukhb, "Coherent anti-Stokes Raman scattering polarized microscopy of three-dimensional director structures in liquid Crystals" *Appl. Phys. Lett*. **91,** 151905(2007).

9. G. S. He, Q. Zheng, N. Cheng, F. Xu, and P. N. Prasad, "Optical phase-conjugation property of three-photon excited stimulated emission," *J. Nonl. Opt. Phys. Mat.* **16,** 137–155 (2007).

10. G. S. He, L.-S. Tan, Q. Zheng, and P. N. Prasad, "Multiphoton absorbing materials: molecular designs, characterizations, and applications" in *Chem. Rev*. **108**, 1245-1330 (2008).

11. G. S. He, Q. Zheng, K.-T. Yong, F. Erogbogbo, M. T. Swihart, and P. N. Prasad, "Two-and three-photon absorption and frequency upconverted emission of silicon quantum dots," *Nano Lett.* **8**, 2688-2692 (2008).

12. G. S. He, K.-T. Yong, H.-Y Qin, Q. zheng, P. N. Prasad, S. He, and H. Agren, "Stimulated Rayleigh-Bragg Scattering From a Two-Photon Absorbing CdSe/Cds/ZnS Quantum-Rods System: Optical Power Limiting and Phase-Conjugation," *IEEE J. Quantum Electron*. **44**, 894-901 (2008).

13. G. S. He, H.-Y. Qin, Q. Zheng, P. N. Prasad, S. Jockusch, N. J. Turro, M. Halim, D. Sames, H. Agren, and S. He, "Dynamic properties and optical phase conjugation of two-photon pumped ultrashort blue stimulated emission in a chromophore solution," *Phys. Rev. A* **77**, 013824 (2008).

14. Q. Zheng, S. K. Gupta, G. S. He, L.-S. Tan, and P. N. Prasad, "Synthesis, characterization, two-photon absorption, and optical limiting properties of ladder-type oligo-p-phenylene-cored chromophores," *Advan. Func. Mat.* **18**, 2770-2779 (2008).

15. Q. Zheng, A. Bonoiu, T. Y. Ohulchanskyy, G. S. He, and P. N. Prasad, "Water-soluble two-photon absorbing nitrosyl complex for light-activated therapy through nitric oxide release," *Molecular Pharmaceutics* **5**, 389-398 (2008).

16. G. S. He, H.-Y. Qin, and Q. Zheng, "Rayleigh, Mie, and Tyndall scatterings of polystyrene microspheres in water: Wavelength, size, and angle dependences**,"** *J. Appl. Phys*. **105**, 023110 (2009).

17. G. S. He, A. P. Zhang, Q. Zheng, H.-Y. Qin, P. N. Prasad, S. He, and H. Ågren, "Multifocus Structures of Ultrashort Self-Focusing Laser Beam Observed in a Three-Photon Fluorescent Medium," *IEEE J. Quantum Electron*. **45**, 816-824 (2009).

18. G. S. He, J. Zhu, K.-T. Yong, R. Hu, Y. Cui, and P. N. Prasad, "Backward stimulated Bragg scattering in multi-photon active $CdTe_xSe_{1-x}$ quantum dots system," *J. Chem. Phys*. **131**, 21430 (2009).

19. G. S. He, K.-T. Yong, J. Z., H.-Y. Qin, and P. N. Prasad, "Two- and three-photon absorption induced emission, optical limiting and stabilization of CdTe/CdS/ZnS quantum tripods system," *IEEE J. Quantum Electron*. 2010 (in press).

20. G. S. He, J. Zhu, K.-T. Yong, A. Baev, H.-X. Cai, R. Hu,[1] Y. Cui, and P. N. Prasad. "Scattering and absorption cross-section spectral measurements of gold-nanorods in water," *J. Phys. Chem. C 2010* (in press).

21. Guang S. He, Ken-Tye Yong, Jing Zhu, and P. N. Prasad, "Stimulated Mie-scattering," (submitted).

22. G. S. He, J. Zhu , P. N. Prasad, L.-S. Tan, R. Kannan, and T. Cooper, "Optical stabilization and temporal reshaping of laser pulse series passing through a nonlinearly absorbing polymer rod," (to be submitted).